Journal of Neurochemistry

JOURNAL OF NEUROCHEMISTRY | 2014 | 129 | 672–682 doi: 10.1111/jnc.12667

ORIGINAL ARTICLE

MRS glucose mapping and PET joining forces: re-evaluation of the lumped constant in the rat brain under isoflurane anaesthesia

Malte F. Alf,*,† João M. N. Duarte,*,‡ Hongxia Lei,*,§ Stefanie D. Krämer,† Vladimir Mlynarik,* Roger Schibli† and Rolf Gruetter*,‡,§

*Laboratory of Functional and Metabolic Imaging, Ecole Polytechnique Fédérale de Lausanne, Lausanne, Switzerland

†Center for Radiopharmaceutical Sciences of ETH Zurich, Zurich, Switzerland

‡Department of Radiology, University of Lausanne, Lausanne, Switzerland

§Department of Radiology, University of Geneva, Geneva, Switzerland

Abstract

Although numerous positron emission tomography (PET) studies with ^{18}F-fluoro-deoxyglucose (FDG) have reported quantitative results on cerebral glucose kinetics and consumption, there is a large variation between the absolute values found in the literature. One of the underlying causes is the inconsistent use of the lumped constants (LCs), the derivation of which is often based on multiple assumptions that render absolute numbers imprecise and errors hard to quantify. We combined a kinetic FDG-PET study with magnetic resonance spectroscopic imaging (MRSI) of glucose dynamics in Sprague–Dawley rats to obtain a more comprehensive view of brain glucose kinetics and determine a reliable value for the LC under isoflurane anaesthesia. Maps of T_{max}/CMR_{glc} derived from MRSI data and T_{max} determined from PET kinetic modelling allowed to obtain an LC-independent CMR_{glc}. The LC was estimated to range from 0.33 ± 0.07 in retrosplenial cortex to 0.44 ± 0.05 in hippocampus, yielding CMR_{glc} between 62 ± 14 and 54 ± 11 μmol/min/100 g, respectively. These newly determined LCs for four distinct areas in the rat brain under isoflurane anaesthesia provide means of comparing the growing amount of FDG-PET data available from translational studies.

Keywords: CMR_{glc}, glucose transport, isoflurane, lumped constant, magnetic resonance spectroscopic imaging, positron emission tomography.

J. Neurochem. (2014) **129**, 672–682.

Cerebral glucose metabolism is linked to neurotransmitter cycling (Sibson *et al.* 1998) and therefore indicative of neuronal activity. It is also known to be altered in various pathologies, such as hypoxia and ischaemia, Alzheimer's and Parkinson's diseases (Hellwig *et al.* 2012; Scheef *et al.* 2012). As energy consumption in the brain is affected by numerous factors, it is all the more desirable to measure it in a fully quantitative fashion to allow for comparison across studies performed under different conditions in different laboratories.

Brain glucose consumption *in vivo* has been determined in a non-invasive way mostly using ^{13}C magnetic resonance spectroscopy (MRS) with infusion of ^{13}C-enriched glucose, ^{1}H MRS upon glycaemia challenges and positron emission tomography (PET) with the glucose analog ^{18}F-fluoro-deoxyglucose (FDG). Notwithstanding its great merits, particularly allowing to determine fluxes through a large number of metabolic reactions, ^{13}C MRS faces limitations regarding spatial resolution. Although ^{1}H MRS has been

Received May 15, 2013; revised manuscript received January 22, 2014; accepted January 24, 2014.

Address correspondence and reprint requests to João M. N. Duarte, EPFL, Laboratory of Functional and Metabolic Imaging, CH F1 625, Station 6, 1015 Lausanne, Switzerland. E-mail: joao.duarte@epfl.ch

Abbreviations used: CMR_{glc}, cerebral metabolic rate of glucose; DG, deoxyglucose; FDG, ^{18}F-fluoro-deoxyglucose; GLUT, glucose transporter; G_p, plasma glucose concentration; K_{FDG}, FDG uptake rate constant; K_t, apparent half-saturation constant for glucose transport; LC, lumped constant; MRSI, magnetic resonance spectroscopic imaging; MRS, magnetic resonance spectroscopy; PET, positron emission tomography; SUV, standard uptake value; T_{max}, apparent maximum transport rate; T_{out}, glucose efflux rate from tissue; V_d, volume of distribution.

mostly restricted to provide information on the ratio of glucose transport over consumption, recent studies have been designed to quantify both transport kinetics and the cerebral metabolic rate of glucose (CMR_{glc}) from the dynamic measurement of brain glucose concentration upon plasma glucose variation (Gruetter *et al.* 1996; Shestov *et al.* 2011; Du *et al.* 2012; Duarte and Gruetter 2012a). PET with FDG offers information on the mechanistic basis of CMR_{glc} and is a relatively uncomplicated method, leading to its widespread employment. However, it is most often used in a semiquantitative manner, reporting standard uptake values rather than calibrated kinetic modelling results (Liu *et al.* 2010; Mizuma *et al.* 2010; Kreissl *et al.* 2011). This has been criticized in the past (Keyes 1995) and is because of two principal issues. The first is the need for a measurement of the FDG concentration in the blood (the so-called input function), which in rodents is complicated by small blood volume. There are commercially available tools for the real-time measurement of the input function in rats (Weber *et al.* 2002) and mice (Alf *et al.* 2013a). The second issue relates to the need of the lumped constant (LC), which accounts for the different affinities of glucose versus its analog, in this case FDG, to glucose transporters and hexokinase and their volumes of distribution. This is particularly needed to derive a value for the consumption of glucose from data describing the uptake of its analog. A good discussion of why the LC is difficult to determine can be found in a perspective article by Krohn *et al.* (2007). Most previous attempts to determine the LC of FDG have been based on an indirect comparison to ^{14}C-DG, for which the LC has been determined in the seminal work in the field (Sokoloff *et al.* 1977), and used operational definitions drawing upon average values for single rate constants from the literature (Tokugawa *et al.* 2007). The latest reported value for the LC in the awake rat for FDG is 0.71 ± 0.12 (Tokugawa *et al.* 2007). Although a large number of FDG-PET studies in rats are performed under isoflurane anaesthesia (*e.g.* Shimoji *et al.* 2004; Backes *et al.* 2011), there is no consensus on the LC to be used in this condition. Recent efforts to calculate LCs for individual animals yielded qualitatively meaningful results but failed to provide realistic values of CMR_{glc} (Backes *et al.* 2011). Overall, there are substantial differences between published results (Table 1) that prohibit comparison between studies from different research groups and suggest a pseudo-quantitative and somewhat arbitrary nature of CMR_{glc} measurements.

Hyder and Rothman (2012) have collected data on CMR_{glc} from rats mostly from ^{13}C MRS studies that suggest a minimum CMR_{glc} of 10–20 μmol/min/100 g to be required to maintain cell viability even at isoelectricity, *i.e.* in the absence of electrical activity that can be reached with deep pentobarbital anaesthesia (Crane *et al.* 1978; Sakabe *et al.* 1985). Although isoflurane has a suppressive effect on neural activity, it has been used in stimulation studies (*e.g.* Barter *et al.* 2005) and it has been demonstrated to only partially reduce haemodynamic signals in rodents at conventionally used doses (*e.g.* Takuwa *et al.* 2012). This suggests that one should expect to find a CMR_{glc} somewhere above 20 μmol/min/100 g but below the consumption level of the awake state that may be even above 100 μmol/min/100 g (Moore *et al.* 2000; Tokugawa *et al.* 2007). Recent studies in mice anaesthetized with isoflurane have reported values of CMR_{glc} as low as 13 and 18 μmol/min/100 g (Mizuma *et al.* 2010; Kreissl *et al.* 2011).

These discrepancies suggest the need for a new determination of the LC under isoflurane anaesthesia. We adopted an entirely new approach to the issue by combining magnetic resonance spectroscopic imaging (MRSI) and PET with FDG to determine T_{max}/CMR_{glc} and T_{max} respectively, in different brain structures. With the standard two-tissue compartment model, this allowed to estimate the actual LC under isoflurane anaesthesia ($LC^{isoflurane}$) without the need of using

Table 1 Values for CMR_{glc} in the cortex (CTX), Hippocampus (HIP) or whole brain (WB) from rodents under isoflurane anaesthesia vary considerably across studies. Except for the first four rows, all results are from FDG-PET studies

Authors	Species	Brain region	Tracer	LC	CMR_{glc} (μmol/min/100 g)
Hansen *et al.* (1989)	Rat	CTX	^{14}C-DG	0.483 (autoradiography)	54 ± 2
		HIP			66 ± 2
Archer *et al.* (1990)	Rat	CTX	^{14}C-DG	0.483 (autoradiography)	37 ± 7 to 48 ± 6
		HIP			42 ± 7 to 63 ± 12
Duarte and Gruetter (2012a)	Rat	CTX+HIP	None	None (dynamic ^{1}H MRS)	54 ± 15
Du *et al.* (2012)	Rat	CTX	None	None (dynamic ^{1}H MRS)	44 ± 17
Shimoji *et al.* (2004)	Rat	CTX	FDG	0.48	23.9 ± 4.8
		WB			28.1 ± 4.6
Backes *et al.* (2011)	Rat	WB	FDG	Derived from kinetics	20 (no SD reported)
Yu *et al.* (2009)	Mouse	CTX	FDG	0.6	40.6 ± 13.3
Mizuma *et al.* (2010)	Mouse	CTX	FDG	0.625	13 ± 4
Kreissl *et al.* (2011)	Mouse	WB	FDG	1	18 (no SD reported)
Alf *et al.* (2012)	Mouse	WB	FDG	0.6	61 ± 11 to 75 ± 24

literature values on the LC for ^{14}C-DG or single rate constants. As there is an ongoing debate on whether it is appropriate to include a rate constant k_4 for dephosphorylation of FDG-6-phosphate, we derived results for both modelling options, *i.e.* with and without k_4 included in the model. The combined information from PET and MRSI also provided a more complete, quantitative description of glucose kinetics in the rat brain. These findings contribute to an improvement in the comparability of quantitative results on brain glucose metabolism.

Materials and methods

All procedures used in the experiments described here were according to the Swiss animal welfare legislation and approved by the local ethics committee and performed by licensed investigators. Male Sprague-Dawley rats for MRSI (253 ± 23 g, n = 10) and PET (304 ± 9 g, n = 6) were purchased from Charles River in France and Germany, respectively, and housed under identical conditions: 12-h light–dark cycle, 20–22°C room temperature, 55–60% humidity, with water and food (Kliba Nafag 3800 from Provimi Kliba) provided *ad libitum*.

Animal preparation

Rats were anaesthetized using 1.5–2% isoflurane in 30% oxygen in air, breathing autonomously at a rate of 60–75 breaths/min. Polyethylene catheters were inserted into a femoral artery and vein. In MRSI experiments, they were used to monitor blood gases, plasma glucose (G_p), and lactate concentrations, and to infuse a 20% (w/v) solution of D-glucose (Sigma-Aldrich, Basel, Switzerland), as described previously (Duarte *et al.* 2009a). In PET experiments, the catheters were connected to form a closed shunt loop with two- to three-way valves in it, for infusion of FDG and G_p monitoring. The shunt was guided through a coincidence counter (twilite, Swisstrace, Switzerland) for the acquisition of real-time input functions with the respective tool in PMOD v3.3 software (PMOD Technologies Inc., Zurich, Switzerland), as described previously (Weber *et al.* 2002; Alf *et al.* 2013a). A peristaltic pump (Ismatec, Wertheim-Mondfeld, Germany) ensured a constant flow rate of 300 μL/min through the shunt.

PET imaging

FDG was administered as an infusion of 200 μL at constant speed over 5 min with a syringe pump. The injected radioactive dose was 31–39 MBq. G_p was measured before, in the middle and after the scan, *i.e.* with 30-min interval. For this purpose, plasma samples were obtained by centrifugation of 40–50 μL whole blood samples and G_p was measured with a glucose oxidase/reflectance system (Vitros DT60 II; Ortho Clinical Diagnostics). Respiratory rate and body temperature were continuously monitored and controlled as described previously (Alf *et al.* 2013a).

List mode PET data acquisition was performed on a GE VISTA eXplore PET/CT system (GE, Fairfield, CT, USA) with 0.9-mm resolution in full width at half maximum in the centre of field of view (Alf *et al.* 2013a,b). Data were collected over 60 min. Animals were killed at the end of the experiment.

Images were reconstructed using a 3D FORE/2D OSEM algorithm to a nominal voxel volume of 0.3875 × 0.3875 × 0.775 (axial) mm^3 as described previously (Alf *et al.* 2013a,b). Time frames were arranged in such a way that the shortest frames (10 s) coincided with the fastest changes in blood concentration of radioactivity, *i.e.* the end of the tracer infusion. The longest frames (4 min) were situated at the end of the scan. In Fig. 2a, each data point of the time activity curve (TAC) stems from one reconstructed time frame.

MR Spectroscopic imaging

Measurements of brain glucose concentrations were performed on a DirectDrive spectrometer (Agilent Technologies, Palo Alto, CA, USA) that was interfaced to an actively shielded 9.4 T magnet with a 31 cm horizontal bore (Magnex Scientific, Abingdon, UK) and with a 12 cm i.d. actively shielded gradient set that allowed a maximum gradient of 400 mT/m in 120 μs. A quadrature coil with two 12-mm-inner-diameter decoupled loops resonating at 400 MHz was used for the radio-frequency transceiver.

We used a standard rectangular k-space acquisition scheme that was accelerated by TR weighting with a 2D-Hamming filter and a circular sampling window as described previously (Kühn *et al.* 1996; Alf *et al.* 2012). Multislice T_2-weighted (TR = 4 s, TE_{eff} = 52 ms, four scans) images were acquired with a fast spin-echo method (Hennig 1988) for positioning of the volume of interest (VOI) for subsequent MRSI scans. A coronally oriented VOI was chosen with dimensions of 6 mm × 9 mm with a thickness of 2.5 mm. SPECIAL (Spin Echo full Intensity Acquired Localized spectroscopy; Mlynárik *et al.* 2008) combined with phase encoding in two dimensions was used for the MRSI metabolite signal acquisition with TE = 2.8 ms and a maximum TR of 2.5 s at the centre of k-space. VAPOR water suppression interleaved with three modules of outer volume saturation was employed. A 32 × 32 k-space data matrix was acquired, covering a field of view of 24 mm × 24 mm. Nominal voxel size was thus 1.4 μL. For the 4 averages acquired, metabolite acquisition time was 90 min and the resulting Cramer-Rao lower bounds of glucose were < 30% also in peripheral voxels, except for a few voxels in the corners and bottom row. After the first MRSI acquisition at baseline G_p, a water reference map (acquisition time of 30 min) was recorded for absolute quantification, while glucose was infused to clamp its plasma concentration to a higher level, as described previously (Duarte and Gruetter 2012a). Once the new G_p was reached, a waiting period of 90 min was observed to ensure for a steady state of glucose transport in the brain, before a second MRSI acquisition was started. The MRSI session took about 5 h altogether: 30 min T_2-weighted scan and shimming, 90 min metabolites, 30 min water (during waiting period), 90 min metabolites. During the whole MRSI session, body temperature, arterial blood pressure, heart rate, and respiratory rate were continuously monitored with an animal monitoring system (SA Instruments, NY, USA). Temperature was maintained at 37.5°C with a warm water circulation system based on the feedback obtained from a rectal temperature probe. Plasma samples collected every 20 min as described above were used to quantify concentrations of glucose and lactate, pH, P_aO_2 and P_aCO_2, as detailed previously (Duarte and Gruetter 2012a).

Data analysis

PET images and input functions were calibrated to kBq/cm^3 by means of a phantom scan with known concentration that was performed daily. With a rat brain template (Schiffer atlas as

implemented in PMOD, Zurich, Switzerland), TACs were generated from the brain structures present in the VOI used for MRSI (Fig. 1a), *i.e.* somatosensory and retrosplenial cortex, hippocampus and thalamus. TACs and input functions were used to perform kinetic modelling with the two-tissue compartment model (Sokoloff *et al.* 1977; Brooks 1982) in PMOD. In brief, the model comprises plasma and tissue compartments and four rate constants that are used to describe FDG metabolism: K_1 (mL/min/cm^3) and k_2 (min^{-1}) represent the rate constants for carrier-mediated transport of FDG from plasma to tissue and back from tissue to plasma respectively; k_3 (min^{-1}) represents the rate constant for FDG phosphorylation by tissue hexokinase; k_4 (min^{-1}) represents the rate constant of FDG dephosphorylation in tissue. In compartment models, K_1 can be seen as a rate constant corrected for the plasma/tissue volume ratio or as the clearance of FDG from plasma (mL/min) per cm^3 tissue. Kinetic modelling was performed with two different variants of the two-tissue compartment model: the first variant included dephosphorylation of FDG-6-phosphate, k_4; the other variant did not include dephosphorylation in the model, *i.e.* irreversible phosphorylation of FDG by hexokinases was assumed. A fractional blood volume of 4.2% was assumed according to synchrotron CT results (Adam *et al.* 2003). Fitting was done with a Levenberg–Marquardt algorithm.

The resulting single rate constants were used to compute the FDG uptake constant (K_{FDG}) and cerebral glucose metabolic rate (CMR_{glc}), for which an initial assumption of $LC^{assumed} = 0.7$ was made, as suggested by the literature for awake rats (Tokugawa *et al.* 2007):

$$K_{FDG} = \frac{K_1 * k_3}{k_2 + k_3} \quad (1)$$

$$CMR_{glc} = \frac{K_{FDG} * G_p}{LC^{assumed}} \quad (2)$$

Glucose transport was calculated with

$$T_{glc} = K_{1,glc} G_p \quad (3)$$

and assumed to be close to the maximum transport velocity (T_{max}) as apparent Michaelis half-saturation constant for glucose transport (K_t below 1.5 mM with reversible Michaelis–Menten kinetics) is much lower than plasma glucose in this study (Duarte and Gruetter 2012a). Thus, T_{max} was estimated according to eqn 4 and then used to determine the ratio of T_{max}/CMR_{glc} for the different brain structures:

$$T_{max} = K_{1,FDG} \times \frac{K_{1,glc}}{K_{1,FDG}} \times \frac{G_p}{1.04\ \text{g/mL}} \quad (4)$$

A tissue density of 1.04 g/mL was assumed. The transport coefficient for FDG versus glucose was $\frac{K_{1,FDG}}{K_{1,glc}} = 1.66$, which is the average of the two available literature values for normoglycemic rats: 1.65 at $G_p = 9$ mM (Fuglsang *et al.* 1986) and 1.67 at $G_p = 9.9$ mM (Crane *et al.* 1983).

Data from MRSI were processed with home-written MATLAB (The MathWorks, Natick, MA, USA) codes as previously detailed (Alf *et al.* 2012) and metabolite quantification was done with LCModel version 6.2-0X (Stephen Provencher Inc., Oakville, Ontario, Canada). MRSI data sets were processed independently from PET images (without coregistration) and regions of interest were manually delineated based on anatomical T_2-weighted MRI scans. As for PET data, a 4.2% fractional blood volume in the brain was taken into account. The glucose distribution volume V_d was fixed at 0.77 mL/g, consistent with the brain water content for absolute quantification (Lund-Andersen 1979). Metabolite maps of glucose were generated, interpolated and superimposed on anatomic images (Fig. 1b).

The reversible Michaelis–Menten model of steady-state glucose kinetics was then applied using eqn 5 (Gruetter *et al.* 1998), which is valid under the range of plasma glucose analysed in this study (Duarte *et al.* 2009b).

$$G_{brain} = V_d \frac{\left(\frac{T_{max}}{CMR_{glc}} - 1\right) G_p - K_t}{\frac{T_{max}}{CMR_{glc}} + 1} \quad (5)$$

As the apparent half-saturation constant for glucose transport at the blood–brain barrier is the poorest estimated parameter when studying glucose dynamics *in vivo* (Duarte *et al.* 2009b), we first proceeded with a fit of eqn 5 to all measured voxels simultaneously. The resulting value for K_t was then used to perform data fitting on all individual voxels. Finally, glucose maps were coregistered to create a map of T_{max}/CMR_{glc} for region-of-interest analysis, analogous to the determination of the ratio from FDG-PET data.

Results from PET and MRSI were then combined to obtain a new, experimental value of the LC as follows. T_{max}/CMR_{glc}

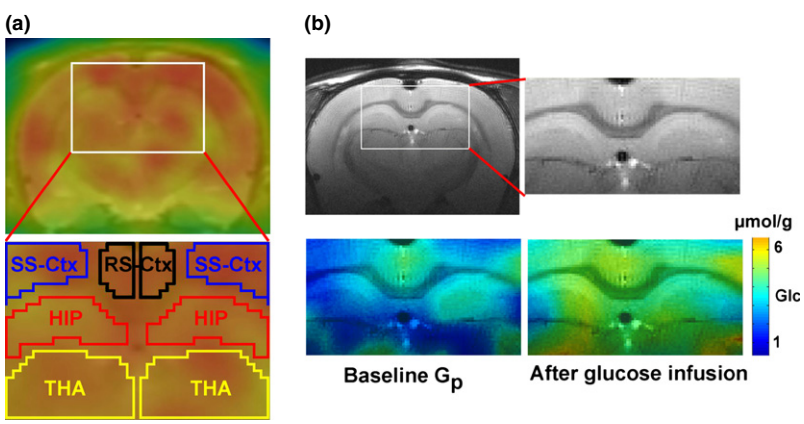

Fig. 1 (a) A typical image of ^{18}F-fluoro-deoxyglucose (FDG) uptake after 45 min. ROIs from which time activity curves (TACs) were derived are shown. Plasma glucose in this animal was 10.7 mmol/L. Delineated brain areas are as follows: SS-Ctx, somatosenory cortex; RS-Ctx, retrosplenial cortex; HIP, hippocampus; THA, thalamus. (b) Typical maps of glucose superimposed on an anatomic MRI scan (top). In the map acquired after glucose infusion, G_p was between 16.5 and 17.8 mmol/L.

determined with either method must be the same, with the LC in the equation for PET being the only parameter free to choose. $LC^{isoflurane}$ can therefore be determined through eqn 6:

$$\frac{\frac{T_{max,PET} * LC^{isoflurane}}{K_{FDG} * G_p}}{\frac{T_{max,MRSI}}{CMR_{glc}}} = 1 \quad (6)$$

which can be written as follows:

$$LC^{isoflurane} = \frac{T_{max,MRSI}}{CMR_{glc}} \times \frac{K_{1,FDG}}{K_{1,glc}} \times \frac{k_3}{k_2 + k_3} \quad (7)$$

After determining $LC^{isoflurane}$, correct values of CMR_{glc} were calculated.

Error propagation was taken into account throughout all layers of analysis. All data are shown with associated SD.

Results

PET kinetic modelling

Of the six rats included in the FDG-PET study, five had a G_p of 10.8 ± 0.5 mmol/L. One rat had a lower initial G_p (7.1 mmol/L) that changed substantially during the scan and was therefore excluded from the analysis. Kinetic model fitting using the two-tissue compartment model as implemented in PMOD could be performed with an excellent data fit in all five data sets (example shown in Fig. 2a), with and without a rate constant for dephosphorylation, k_4, included in the model. Results for the rate constants, the CMR_{glc} (determined with LC = 0.7) and T_{max} are shown in Table 2. T_{max} revealed significant regional variations, with the value in retrosplenial cortex being significantly higher than that in hippocampus (with model including k_4: 149 ± 23 vs. 105 ± 16 μmol/min/100 g, model excluding k_4: 152 ± 20 vs. 108 ± 13; $n = 5$, $p < 0.05$, two-tailed paired-sample t-test). CMR_{glc} was relatively uniform with differences below 10% across different brain regions when calculated with an LC of 0.7 in all regions. T_{max}/CMR_{glc} was calculated and is shown in Table 3. The rate constant for dephosphorylation, k_4, was found to be close to zero, with its SD being larger than its absolute value. Omitting k_4 from the analysis did not lead to significantly different results.

Parameters from MRSI

Physiologic parameters of the animals used for MRSI are summarized in Table 4. Plasma lactate increased when G_p was increased via glucose infusion. This was also visible in brain lactate maps (not shown). As in previous reports on single volume MRS data (Duarte *et al.* 2009a; Duarte and Gruetter 2012a), we did not observe major changes in metabolites other than glucose and lactate. A few maps had to be discarded because of issues with poor signal-to-noise ratio or lipid contamination. In the remaining data sets,

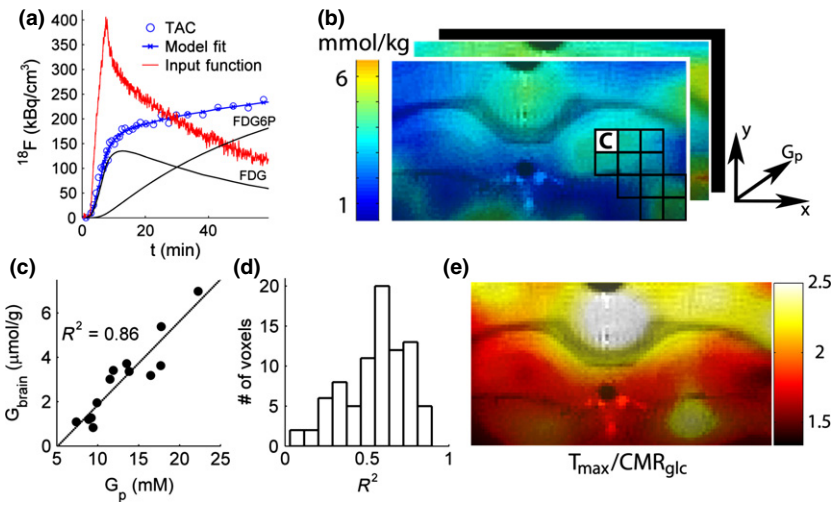

Fig. 2 (a) Typical hippocampal time activity curve (TAC, circles correspond to the centres of reconstructed time frames) and input function from a positron emission tomography PET experiment with model fit. The *y*-axis shows total ^{18}F activity from ^{18}F-fluoro-deoxyglucose (FDG) and FDG-6-phosphate (FDG6P). The black lines represent the intracellular pools of free FDG and FDG6P simulated with the software PMOD. These plus the plasma FDG (red line) within brain capillaries result in the total PET signal (shown in blue). (b) Glucose maps were coregistered for single-voxel regression analysis. A voxel size is illustrated in the lower right corner of the map in front. (c) Data recorded from the voxel highlighted in figure part b from all animals. Linear regression constrained by K_t = 2.1 mmol/L on data from an example voxel, highlighted in (b) in white. (d) Quality of regression as indicated by R^2 for all voxels included in the map. (e) Regression results for T_{max}/CMR_{glc} visualized in a heat map.

Table 2 Results from two-tissue compartment modelling of FDG-PET data, including or excluding k_4 in the model. T_{max} was calculated as described in eqn 4. The values of CMR_{glc} presented in this table were calculated with LC = 0.7 as an initial assumption that would only be correct in awake animals. Brain areas are as follows: SS-Ctx, somatosenory cortex; RS-Ctx, retrosplenial cortex; HIP, hippocampus; THA, thalamus

	K_1 (mL/min/cm^3)	k_2 (min^{-1})	k_3 (min^{-1})	k_4 (min^{-1})	K_{FDG} (mL/min/cm^3)	CMR_{glc} (μmol/min/100 g)	T_{max} (μmol/min/100 g)
Model including k_4							
RS-CTX	0.24 ± 0.03	0.43 ± 0.04	0.04 ± 0.01	0.003 ± 0.008	0.020 ± 0.002	29.3 ± 3.4	149 ± 23
SS-CTX	0.21 ± 0.03	0.42 ± 0.07	0.05 ± 0.01	0.004 ± 0.004	0.021 ± 0.002	30.8 ± 3.4	128 ± 19
HIP	0.17 ± 0.02	0.34 ± 0.09	0.05 ± 0.02	0.005 ± 0.009	0.023 ± 0.005	34.0 ± 6.0	105 ± 16
THA	0.20 ± 0.04	0.40 ± 0.08	0.05 ± 0.01	0.005 ± 0.007	0.021 ± 0.003	31.6 ± 4.7	123 ± 27
Model excluding k_4							
RS-CTX	0.24 ± 0.03	0.44 ± 0.05	0.04 ± 0.01		0.019 ± 0.003	28.1 ± 4.1	152 ± 20
SS-CTX	0.21 ± 0.02	0.43 ± 0.03	0.04 ± 0.01		0.020 ± 0.002	29.0 ± 3.1	132 ± 10
HIP	0.17 ± 0.02	0.34 ± 0.05	0.05 ± 0.01		0.021 ± 0.002	31.3 ± 2.2	108 ± 13
THA	0.20 ± 0.03	0.40 ± 0.05	0.04 ± 0.01		0.020 ± 0.001	29.7 ± 2.8	123 ± 21

Table 3 Summary of glucose transport and consumption results obtained with the combined PET-MRSI analysis. Tissue glucose concentration G_{brain} was calculated at G_p = 10.8 mmol/L (average for animals in the PET study) with two different approaches. Results are shown for models including and excluding k_4 as in the original publication of the two-tissue compartment model (Sokoloff *et al.* 1977). Brain areas are as follows: SS-CTX, somatosenory cortex; RS-CTX, retrosplenial cortex; HIP, hippocampus; THA, thalamus

		RS-CTX	SS-CTX	HIP	THA
	T_{max}/CMR_{glc} (from MRS)	2.5 ± 0.1	2.2 ± 0.1	2.0 ± 0.1	2.0 ± 0.1
	G_{brain} (μmol/g, from MRS)	3.1 ± 0.1	2.6 ± 0.1	2.2 ± 0.1	2.1 ± 0.1
Model with k_4	T_{max}/CMR_{glc} (from PET)	5.1 ± 1.0	4.2 ± 0.4	3.1 ± 0.3	3.9 ± 0.4
	$LC_{isoflurane}$	0.33 ± 0.07	0.37 ± 0.04	0.44 ± 0.05	0.35 ± 0.04
	CMR_{glc} (μmol/min/100 g)	62 ± 14	58 ± 12	54 ± 11	63 ± 12
Model without k_4	T_{max}/CMR_{glc} (from PET)	5.4 ± 0.6	4.6 ± 0.6	3.4 ± 0.4	4.2 ± 0.6
	$LC_{isoflurane}$	0.32 ± 0.03	0.33 ± 0.04	0.40 ± 0.04	0.33 ± 0.05
	CMR_{glc} (μmol/min/100 g)	62 ± 10	61 ± 7	55 ± 4	63 ± 6

Table 4 Average physiologic parameters during baseline and hyperglycaemia clamp in MRSI. P_aO_2 was relatively high because of the mixture of 30% pure oxygen in air. Baseline plasma glucose ranged from 7.4 to 13.8 mmol/L, under glucose clamp conditions from 16.5 to 22.6 mmol/L

	Arterial pH	P_aCO_2 (mm Hg)	P_aO_2 (mm Hg)	O_2 saturation	Plasma lactate (mM)
Baseline[a]	7.36 ± 0.04	43.0 ± 2.0	245 ± 42	99.8 ± 0.1%	2.2 ± 0.6
Glucose clamp	7.31 ± 0.07	38.8 ± 3.7	280 ± 75	99.9 ± 0.1%	4.8 ± 0.9

[a]These parameters were not measured during PET experiments as these lasted only 60 min and no changes were expected.

single-voxel signal to noise ratio was 5–24 and Cramer-Rao lower bounds of glucose concentration were between 6% and 29%, as estimated by LCModel (Stephen Provencher Inc). A total of 13 maps of glucose concentration at different G_p were used to determine a general value for K_t and then to generate the brain map of T_{max}/CMR_{glc} in the voxel-wise regression analysis, as described in the methods section. In agreement with our previous dynamic ^{1}H MRS study (Duarte and Gruetter 2012a; that revealed K_t 1.5 mmol/L (95% CI: 0; 17)), an overall K_t of 2.1 ± 0.6 mmol/L (95% CI: 1.1; 3.1) along with an overall T_{max}/CMR_{glc} of 2.0 ± 0.1 (95% CI: 1.9; 2.1) resulted in the best fit (R^2 = 0.46) of the reversible Michaelis–Menten model. Using this value for K_t, high R^2 were obtained for most fits of individual voxel data (Fig. 2b–d). Voxels with fits resulting in $R^2 < 0.5$ were all situated in either corners of the map or its bottom row. The regional distribution of T_{max}/CMR_{glc} is shown in Fig. 2e. T_{max}/CMR_{glc} ranged from 1.8 in voxels of the hippocampus or thalamus to 2.5 in the retrosplenial cortex. Mean values for the brain areas in the map, *i.e.* retrosplenial cortex, somatosensory cortex, hippocampus and thalamus, were then computed without including voxels of the sinus and the corners (Table 3). G_{brain} for G_p = 10.8

mmol/L (PET study average) was then estimated using eqn 5 and the parameters for the different structures. Values were between 2.1 and 3.1 μmol/g (Table 3).

Estimation of $LC^{isoflurane}$

Compared to MRSI, the ratio T_{max}/CMR_{glc} was overestimated by PET with a factor around 2, when based on the initially assumed LC of 0.7. As a consequence, the actual $LC^{isoflurane}$ must be about half of the initial assumption. Region-specific values for the LC were derived using eqn 6 (Table 3). The highest $LC^{isoflurane}$ of 0.44 ± 0.05 (k_4 included in kinetic model, 0.40 when k_4 was excluded) was obtained in hippocampus, which was significantly higher than the $LC^{isoflurane}$ obtained in the other regions ($p < 0.05$, one-way ANOVA), with the other ones being relatively similar (0.33 ± 0.07, 0.37 ± 0.04 and 0.35 ± 0.04 for retrosplenial and somatosensory cortex and thalamus respectively; with k_4 excluded from the model: 0.32 ± 0.03, 0.33 ± 0.04, 0.33 ± 0.05).

When computed with the $LC^{isoflurane}$ determined in this study, CMR_{glc} was between 54 and 63 μmol/min/100 g in hippocampus and thalamus, respectively, with no major dependence on whether k_4 was included in PET kinetic modelling or not (Table 3).

Discussion

The combination of PET and ^{1}H MRSI was used to determine region-specific LC values in the rat brain under isoflurane anaesthesia. $LC^{isoflurane}$ in the four analysed brain areas was lower than those previously reported for both anaesthetized and awake animals (Table 1), and yielded CMR_{glc} values that are close to those determined by autoradiography (Hansen *et al.* 1989; Archer *et al.* 1990), as well as by LC-independent MRS (Du *et al.* 2012; Duarte and Gruetter 2012a).

The present approach to estimate LC relies on knowing the maximum glucose transport rate (T_{max}) determined by FDG-PET and on its ratio to glucose consumption (T_{max}/CMR_{glc}) measured by ^{1}H MRSI. Both T_{max} and T_{max}/CMR_{glc} reported in this study were in good agreement with previous determinations in the rat brain under isoflurane anaesthesia by dynamic measurement of brain and plasma glucose concentrations (Du *et al.* 2012; Duarte and Gruetter 2012a).

To allow estimating LC, non-measured parameters were taken from the literature. Since they apply to calculations in both MRSI and PET data, such assumptions are devoid of substantial effects on the calculated LC values. Namely, the volume of distribution of glucose in the brain was assumed to be equal to brain water content (Lund-Andersen 1979) and a value for fractional blood volume was taken from synchrotron radiation CT data (Adam *et al.* 2003). It is also implicit in the present analysis that glucose homeostasis is identical in MRSI and PET experiments, *i.e.* that glucose transport and consumption are invariable within the range of plasma glucose concentrations of this study, and are not substantially affected by the presence of FDG in tracer amounts. Indeed, variations in glucose transport and phosphorylation rates were negligible in the mouse brain within the glycaemia range of the present experiments (Alf *et al.* 2013b). In contrast, assumptions that may affect either MRSI or PET data independently are discussed below.

The present FDG-PET data were analysed with two model variants assuming reversible and irreversible phosphorylation. They yielded similar results (within the reported SD). The difference in $LC^{isoflurane}$ was at most 12% (somatosensory cortex). An earlier study in conscious rats using ^{14}C-DG found that the inclusion of k_4 in the CMR_{glc} calculation may lead to a 44% overestimation of CMR_{glc} (Schmidt *et al.* 1995). Such overestimation of CMR_{glc} was not observed in our study under isoflurane. The contrast between the two studies may arise from the effects of isoflurane in the regulation of brain glucose homeostasis, which are not present in awake animals, as well as from the employment of different glucose analogs (^{14}C-DG vs. FDG).

Estimation of K_t and T_{max}/CMR_{glc} from MRSI data

The apparent half-saturation constant for glucose transport into brain parenchyma (K_t) was 2.1 ± 0.6 mmol/L, in agreement with our earlier work using the reversible Michaelis–Menten kinetics for glucose carriers (Duarte and Gruetter 2012a). This is, however, a parameter that varies considerably in the literature as it depends on the kinetic model attributed to the glucose carrier at the blood–brain barrier. The employment of the reversible Michaelis–Menten kinetics to describe glucose transport at the blood–brain barrier resulted in a K_t lower than that determined using the standard Michaelis–Menten model in earlier studies (comparison in Duarte and Gruetter 2012b). In this study, K_t was determined with data pooled from all analysed voxels to achieve higher precision and then constrained for the determination of T_{max}/CMR_{glc} in a voxel-wise manner. With K_t fixed at 2.1 mmol/L for all brain regions, we measured higher T_{max}/CMR_{glc} in cortical tissue, especially in the retrosplenial cortex (Fig. 2e), which may be partly owing to pial vessels contributing to a higher fractional blood volume in this region, compared to the underlying tissue (Chugh *et al.* 2009). Although voxels of the sinus were not included in the analysis, partial volume effects causing signal spill over would lead to overestimation of T_{max}/CMR_{glc} and thus $LC^{isoflurane}$. This artefact may be considered negligible as, slightly higher T_{max}/CMR_{glc} was indeed found in the rat cortex (Lei *et al.* 2010) compared to the hippocampus (Duarte *et al.* 2009a), and CMR_{glc} is generally lower in the cortex than hippocampus (Table 1).

Although the physiological variation of K_t within the analysed brain regions cannot be excluded, simulations of the effect of K_t on T_{max}/CMR_{glc} and thus on LC estimation (Fig. 3a) indicated that variations of 50% in the value of K_t

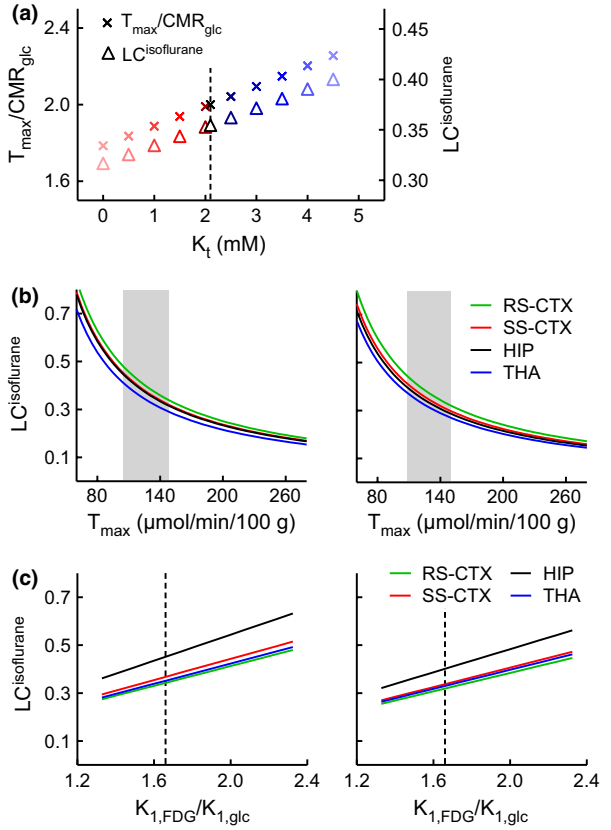

Fig. 3 (a) Simulation of the effect of K_t on the determination of T_{max}/CMR_{glc} from magnetic resonance spectroscopic imaging (MRSI) data and, consequently, on the estimation of $LC^{isoflurane}$, using ^{18}F-fluoro-deoxyglucose (FDG)-PET rate constants averaged across the four brain regions (model including k_4). The experimentally determined K_t = 2.1 mM is represented by the dashed line. (b) Effect of T_{max} estimated from FDG-PET data on $LC^{isoflurane}$. The shaded area represents the values of T_{max} obtained experimentally in this study for the regions of interest. (c) Effect of varying $K_{1,FDG}/K_{1,glc}$ on the determination of T_{max}/CMR_{glc} and/or $LC^{isoflurane}$. The dashed vertical line represents the value assumed for LC estimation. Regions of interest are as follows: RS-CTX, retrosplenial cortex; SS-CTX, somatosenory cortex; HIP, hippocampus; THA, thalamus. On panels (b) and (c), right and left graphs are simulations with FDG-PET rate constants in models with and without k_4, respectively.

resulted in changes in the $LC^{isoflurane}$ (and T_{max}/CMR_{glc}) smaller than 6%. An increase in $LC^{isoflurane}$ of 11% was found when doubling the value of K_t to 4.2 mmol/L, which is higher than any estimation with the reversible Michaelis–Menten model of glucose carriers across different species (Duarte and Gruetter 2012b).

Rate constants and T_{max} from FDG-PET data

K_t in the rat brain *in vivo* determined from MRSI data was much lower than plasma glucose in the animals used for PET experiments. As such, we assumed that glucose transport (T_{glc}) estimated from K_1 is close to T_{max}. The values for T_{max} obtained in this manner (105–152 μmol/min/100 g) were close to the T_{max} of 137 μmol/min/100 g obtained for the rat brain (cortex+hippocampus) in a ^{1}H MRS study under similar anaesthesia protocol (Duarte and Gruetter 2012a) and in line with LC-independent measurements of T_{max} under different experimental conditions, ranging from 91 to 135 μmol/min/100 g (Duarte *et al.* 2011; Du *et al.* 2012). As this assumption may result in underestimating T_{max} from PET data, we simulated the effect of T_{max} on $LC^{isoflurane}$ (Fig. 3b), which indicated that a 20% increase in T_{max} estimated from PET experiments (relative to values on Table 2) would result in 17–18% decrease in $LC^{isoflurane}$ in the four regions of interest analysed.

Furthermore, since K_1 for glucose ($K_{1,glc}$) was not measured, the estimation of T_{max} from PET data relied on previous determinations of the coefficient of transport rate constants $K_{1,FDG}/K_{1,glc}$ that was 1.66 for adult rats at a glycaemia of 9–10 mM (Crane *et al.* 1983; Fuglsang *et al.* 1986), not substantially different from the present FDG-PET study (10.8 ± 0.5 mmol/L). The value of $K_{1,FDG}/K_{1,glc}$ used in this study seems to be appropriate as it draws upon two independently achieved results from the literature that differ < 2% from each other, and also K_1 remains unchanged relative to awake rats *in vivo* (Mizuma *et al.* 2010). Nevertheless, care should be taken when extrapolating the present data to other experimental conditions where $K_{1,FDG}/K_{1,glc}$ may vary, as it was shown for newborn rats (increase of ~16%; Fuglsang *et al.* 1986). In humans, $K_{1,FDG}/K_{1,glc}$ was 1.48 and did not change under hypo- or hyperglycaemia (Hasselbalch *et al.* 1996).

Simulations with the data from our study indicated that variations of $K_{1,FDG}/K_{1,glc}$ have a proportional effect on the estimated LC. For the sake of example, a variation of 10% in $K_{1,FDG}/K_{1,glc}$ in the somatosensory cortex (between 1.49 and 1.83) resulted in LC to vary between 0.33 and 0.41 (model including or not k_4), which is within the associated variance (Fig. 3c).

Based on previous work measuring brain glucose concentrations in a vast range of experimental conditions with both microdialysis and MRS methods (reviewed in Barros *et al.* 2007; Duarte and Gruetter 2012b), we consider that G_{brain} as assessed with MRSI reflects its true value in the present work. Thus, with the measured values of G_{brain} by MRSI and the calculated CMR_{glc}, one can estimate a coefficient of phosphorylation rate constants $\frac{k3,FDG}{k3,glc}$, as defined by Crane *et al.* (1983), using an expression similar to eqn 1:

$$CMR_{glc} = k_{3,FDG}\frac{k_{3,glc}}{k_{3,FDG}}G_{brain} \times 1.04\,\text{g/mL} \qquad (8)$$

This analysis resulted in $\frac{k_{3,FDG}}{k_{3,glc}}$ ranging from 0.17 to 0.23 across the four regions of interest. This is lower than the coefficient obtained in other studies in rats with FDG (0.50–0.55; Crane *et al.* 1983; Fuglsang *et al.* 1986) or

deoxyglucose (0.37; Cunningham and Cremer 1981), in agreement with the lower LC values determined in this study. In this context, it should be noted that isoflurane substantially decreases k_3 itself relative to the awake state in the mouse brain (Mizuma *et al.* 2010).

Despite the mentioned shortcomings, our approach represents a solid basis compared to strategies that rely on additional assumptions included in operational definitions and/or hexokinase affinities or single rate constants from the literature. We therefore argue that the explanation of why our $LC^{isoflurane}$ is lower than in previous reports is likely to be found in these additional assumptions.

Physiological effects of isoflurane

In this study, we report LC values that may not be applicable to experiments under anaesthesia protocols other than the widely used isoflurane. Isoflurane influences brain and peripheral metabolism, particularly increasing brain and plasma lactate and glucose levels (Saha *et al.* 2005; Duarte and Gruetter 2012a; Boretius *et al.* 2013). These did not vary during the time frame of the present PET and MRSI measurements. As we use a glycaemic clamp to control for plasma glucose after the first half of the MRSI session, we do not expect the influence of isoflurane on plasma glucose to be of importance. Although CMR_{glc} has been found to be similar in the rat brain under α-chloralose and isoflurane anaesthesia (Duarte *et al.* 2011; Duarte and Gruetter 2012a), that are characterized by distinct plasma and brain lactate levels, influence of lactate on other brain metabolic processes would benefit from further research. Another effect of isoflurane anaesthesia is that it makes CMR_{glc} more uniform across the brain than it is in the awake state, as discussed previously (Toyama *et al.* 2004) and as visible in our data. This does not prohibit its use in most experimental protocols, as long as it is kept in mind. However, in addition to the above-mentioned effects, it further precludes our results from being transferable to experiments with other types of anaesthesia or in the awake state.

Experimental limitations

In MRSI, slight differences were observed between the left and right hemispheres. These are probably owing to partial volume effects, a generalized problem in MR imaging and particularly in MRSI (discussed in Alf *et al.* 2012). The real voxel size of the glucose maps (1.4 μL) is relatively large compared to the size of brain structures, resulting in voxels that are weighted averages of spectra containing different brain structures. This kind of image artefacts could be reduced by developing MRSI methods with higher spatial resolution, but with loss in the signal-to-noise ratio within the same acquisition time, which is important when quantifying low concentrated metabolites like glucose.

It should also be noted that distinct animals were used for the MRSI and PET experiments, although strain and housing conditions were identical, thus minimizing metabolic and physiological variations. The rats were 7 and 8 weeks old for PET and MRSI, respectively, and this age difference has not been demonstrated to have an effect on brain energy metabolism, to our knowledge. Nevertheless, more reliable estimations of LC can be envisaged by employment of newly developed instruments that combine both imaging methods (Torigian *et al.* 2013) for simultaneous FDG-PET and dynamic ^{13}C MRS with infusion of ^{13}C-enriched glucose as the latter provides independent measures of T_{max}, CMR_{glc} and K_t (Duarte *et al.* 2011).

Conclusion

This study reports region-specific values for the FDG LC in the rat brain under isoflurane anaesthesia that were estimated with as few assumptions as possible. Our results suggest that the ratio of the affinities of hexokinase for glucose and FDG may be decreased under isoflurane compared to the awake state or, possibly, under other anaesthetic agents, which could explain why previous attempts to determine the LC have not resulted in its correct assessment. These region-specific LC values may contribute to a better comparability of quantitative assessments of cerebral energy metabolism using FDG-PET.

Acknowledgments and conflict of interest disclosure

This work was supported (MFA) by the Swiss National Competence Center for Biomedical Imaging (NCCBI). JMND, VM and RG were funded by the Centre d'Imagerie BioMédicale (CIBM) of the UNIL, UNIGE, HUG, CHUV, EPFL and the Leenaards and Jeantet Foundations.

All experiments were conducted in compliance with the ARRIVE guidelines. The authors have no conflict of interest to declare.

References

Adam J. F., Elleaume H., Le Duc G., Corde S., Charvet A. M., Troprès I., Le Bas J. F. and Estève F. (2003) Absolute cerebral blood volume and blood flow measurements based on synchrotron radiation quantitative computed tomography. *J. Cereb. Blood Flow Metab.* **23**, 499–512.

Alf M. F., Lei H., Berthet C., Hirt L., Gruetter R. and Mlynárik V. (2012) High-resolution spatial mapping of changes in the neurochemical profile after focal ischemia in mice. *NMR Biomed.* **25**, 247–254.

Alf M. F., Wyss M. T., Weber B., Buck A., Schibli R. and Krämer S. D. (2013a) Quantification of brain glucose metabolism by FDG PET with real-time arterial and image-derived input function in mice. *J. Nucl. Med.* **54**, 132–138.

Alf M. F., Duarte J. M. N., Schibli R., Gruetter R. and Krämer S. D. (2013b) Brain glucose transport and phosphorylation under acute insulin-induced hypoglycemia in mice: an FDG PET study. *J. Nucl. Med.* **54**, 2153–2160.

Archer D. P., Elphinstone M. G. and Pappius H. M. (1990) The effect of pentobarbital and isoflurane on glucose metabolism in

thermally injured rat brain. *J. Cereb. Blood Flow Metab.* **10**, 624–630.

Backes H., Walberer M., Endepols H., Neumaier B., Graf R., Wienhard K. and Mies G. (2011) Whiskers area as extracerebral reference tissue for quantification of rat brain metabolism using ^{18}F-FDG PET: application to focal cerebral ischemia. *J. Nucl. Med.* **52**, 1252–1260.

Barros L. F., Bittner C. X., Loaiza A. and Porras O. H. (2007) A quantitative overview of glucose dynamics in the gliovascular unit. *Glia* **55**, 1222–1237.

Barter L., Dominguez C. L., Carstens E. and Antognini J. F. (2005) The effect of isoflurane and halothane on electronencephalographic activation elicited by repetitive noxious c-fiber stimulation. *Neurosci. Letters* **3**, 242–247.

Boretius S., Tammer R., Michaelis T., Brockmöller J. and Frahm J. (2013) Halogenated volatile anesthetics alter brain metabolism as revealed by proton magnetic resonance spectroscopy of mice in vivo. *NeuroImage* **69**, 244–255.

Brooks R. A. (1982) Alternative formula for glucose utilization using labeled deoxyglucose. *J. Nucl. Med.* **23**, 538–539.

Chugh B. P., Lerch J. P., Yu L. X., Pienkowski M., Harrison R. V., Henkelman R. M. and Sled J. G. (2009) Measurement of cerebral blood volume in mouse brain regions using micro-computed tomography. *NeuroImage* **47**, 1312–1318.

Crane P. D., Braun L. D., Cornford E. M., Cremer J. E., Glass J. M. and Oldendorf W. H. (1978) Dose dependent reduction of glucose utilization by pentobarbital in rat brain. *Stroke* **9**, 12–18.

Crane P. D., Pardridge W. M., Braun L. D. and Oldendorf W. H. (1983) Kinetics of transport and phosphorylation of 2-fluoro-2-deoxy-D-glucose in rat brain. *J. Neurochem.* **40**, 160–167.

Cunningham V. J. and Cremer J. E. (1981) A method for the simultaneous estimation of regional rates of glucose influx and phosphorylation in rat brain using radiolabeled 2-deoxyglucose. *Brain Res.* **221**, 319–330.

Du F., Zhang Y., Zhu X. H. and Chen W. (2012) Simultaneous measurement of glucose blood-brain transport constants and metabolic rate in rat brain using *in-vivo* ^{1}H MRS. *J. Cereb. Blood Flow Metab.* **32**, 1778–1787.

Duarte J. M. N. and Gruetter R. (2012a) Characterization of cerebral glucose dynamics *in vivo* with a four-state conformational model of transport at the blood-brain barrier. *J. Neurochem.* **121**, 396–406.

Duarte J. M. N. and Gruetter R. (2012b) in neural metabolism *in vivo*, in *Cerebral Glucose Transport and Homeostasis* (Choi I.-Y. and Gruetter R., eds), pp. 655–673. Springer, New York.

Duarte J. M. N., Carvalho R. A., Cunha R. A. and Gruetter R. (2009a) Caffeine consumption attenuates neurochemical modifications in the hippocampus of streptozotocin-induced diabetic rats. *J. Neurochem.* **111**, 368–379.

Duarte J. M. N., Morgenthaler F. D., Lei H., Poitry-Yamate C. and Gruetter R. (2009b) Steady-state brain glucose transport kinetics re-evaluated with a four-state conformational model. *Front. Neuroenergetics* **1**, 6.

Duarte J. M. N., Lanz B. and Gruetter R. (2011) Compartmentalised cerebral metabolism of [1,6-^{13}C]glucose determined by *in vivo* ^{13}C NMR spectroscopy at 14.1 T. *Front. Neuroenergetics* **3**, 3

Fuglsang A., Lomholt M. and Gjedde A. (1986) Blood-brain transfer of glucose and glucose analogs in newborn rats. *J. Neurochem.* **46**, 1417–1428.

Gruetter R., Novotny E. J., Boulware S. D., Rothman D. L. and Shulman R. G. (1996) ^{1}H NMR studies of glucose transport in the human brain. *J. Cereb. Blood Flow Metab.* **16**, 427–438.

Gruetter R., Ugurbil K. and Seaquist E. R. (1998) Steady-state cerebral glucose concentrations and transport in the human brain. *J. Neurochem.* **70**, 397–408.

Hansen T. D., Warner D. S., Todd M. M. and Vust L. J. (1989) The role of cerebral metabolism in determining the local cerebral blood flow effects of volatile anesthetics: evidence for persistent flow-metabolism coupling. *J. Cereb. Blood Flow Metab.* **9**, 323–328.

Hasselbalch S. G., Knudsen G. M., Holm S., Hageman L. P., Capaldo B. and Paulson O. B. (1996) Transport of D-glucose and 2-fluorodeoxyglucose across the blood-brain barrier in humans. *J. Cereb. Blood Flow Metab.* **16**, 659–666.

Hellwig S., Amtage F., Kreft A. *et al.* (2012) [^{18}F]FDG-PET is superior to [123I]IBZM-SPECT for the differential diagnosis of parkinsonism. *Neurology* **79**, 1314–1322.

Hennig J. (1988) Multiecho imaging sequences with low refocusing flip angles. *J. Magn. Reson.* **78**, 397–407.

Hyder F. and Rothman D. L. (2012) Quantitative fMRI and oxidative neuroenergetics. *NeuroImage* **62**, 985–994.

Keyes J. W., Jr (1995) SUV: standard uptake or silly useless value? *J. Nucl. Med.* **36**, 1836–1839.

Kreissl M. C., Stout D. B., Wong K. P. *et al.* (2011) Influence of dietary state and insulin on myocardial, skeletal muscle and brain [^{18}F]-fluorodeoxyglucose kinetics in mice. *EJNMMI Res.* **1**, 8.

Krohn K. A., Muzi M. and Spence A. M. (2007) What is in a number? The FDG lumped constant in the rat brain. *J. Nucl. Med.* **48**, 5–7.

Kühn B., Dreher W., Norris D. G. and Leibfritz D. (1996) Fast proton spectroscopic imaging employing k-space weighting achieved by variable repetition times. *Magn. Reson. Med.* **35**, 457–464.

Lei H., Duarte J. M. N., Mlynarik V., Python A. and Gruetter R. (2010) Deep thiopental anesthesia alters steady-state glucose homeostasis but not the neurochemical profile of rat cortex. *J. Neurosci. Res.* **88**, 413–419.

Liu Y. R., Cardamone L., Hogan R. E. *et al.* (2010) Progressive metabolic and structural cerebral perturbations after traumatic brain injury: An *in vivo* imaging study in the rat. *J. Nucl. Med.* **51**, 1788–1795.

Lund-Andersen H. (1979) Transport of glucose from blood to brain. *Physiol. Rev.* **59**, 305–352.

Mizuma H., Shukuri M., Hayashi T., Watanabe Y. and Onoe H. (2010) Establishment of *in vivo* brain imaging method in conscious mice. *J. Nucl. Med.* **51**, 1068–1075.

Mlynárik V., Kohler I., Gambarota G., Vaslin A., Clarke P. G. and Gruetter R. (2008) Quantitative proton spectroscopic imaging of the neurochemical profile in rat brain with microliter resolution at ultra-short echo times. *Magn. Reson. Med.* **59**, 52–58.

Moore A. H., Osteen C. L., Chatziioannou A. F., Hovda D. A. and Cherry S. R. (2000) Quantitative assessment of longitudinal metabolic changes *in vivo* after traumatic brain injury in the adult rat. *J. Cereb. Blood Flow Metab.* **20**, 1492–1501.

Saha J. K., Xia J., Grondin J. M., Engle S. K. and Jakubowski J. A. (2005) Acute hyperglycemia induced by ketamine/xylazine anaesthesia in rats: mechanisms and implications for preclinical models. *Exp. Biol. Med. (Maywood)* **230**, 777–784.

Sakabe T., Tsutsui T., Maekawa T., Ishikawa T. and Takeshita H. (1985) Local cerebral glucose utilization during nitrous oxide and pentobarbital anaesthesia in rats. *Anesthesiology* **63**, 262–266.

Scheef L., Spottke A., Daerr M. *et al.* (2012) Glucose metabolism, gray matter structure, and memory decline in subjective memory impairment. *Neurology* **79**, 1332–1339.

Schmidt K. C., Mies G., Dienel G. A., Cruz N. F., Crane A. M. and Sokoloff L. (1995) Analysis of time courses of metabolic precursors and products in heterogeneous rat brain tissue: limitations of kinetic modeling for predictions of intracompartmental concentrations from total tissue activity. *J. Cereb. Blood Flow Metab.* **15**, 474–484.

Shestov A. A., Emir U. E., Kumar A., Henry P. G., Seaquist E. R. and Oz G. (2011) Simultaneous measurement of glucose transport and

utilization in the human brain. *Am. J. Physiol. Endocrinol. Metab.* **301**, E1040–E1049.

Shimoji K., Ravasi L., Schmidt K., Soto-Montenegro M. L., Esaki T., Seidel J., Jagoda E., Sokoloff L., Green M. V. and Eckelman W. C. (2004) Measurement of cerebral glucose metabolic rates in the anesthetized rat by dynamic scanning with ^{18}F-FDG, the ATLAS small animal PET scanner, and arterial blood sampling. *J. Nucl. Med.* **45**, 665–672.

Sibson N. R., Dhankhar A., Mason G. F., Rothman D. L., Behar K. L. and Shulman R. G. (1998) Stoichiometric coupling of brain glucose metabolism and glutamatergic neuronal activity. *Proc. Natl Acad. Sci. USA* **95**, 316–321.

Sokoloff L., Reivich M., Kennedy C., Des Rosiers M. H., Patlak C. S., Pettigrew K. D., Sakurada O. and Shinohara M. (1977) The [^{14}C] Deoxyglucose method for the measurement of local cerebral glucose utilization: theory, procedure, and normal values in the conscious and anesthetized albino rat. *J. Neurochem.* **28**, 897–916.

Takuwa H., Matsuura T., Obata T., Kawaguchi H., Kanno I. and Ito H. (2012) Hemodynamic changes during somatosensory stimulation in awake and isoflurane-anesthetized mice measured by laser-Doppler flowmetry. *Brain Res.* **1472**, 107–112.

Tokugawa J., Ravasi L., Nakayama T., Schmidt K. C. and Sokoloff L. (2007) Operational lumped constant for FDG in normal adult male rats. *J. Nucl. Med.* **48**, 94–99.

Torigian D. A., Zaidi H., Kwee T. C., Saboury B., Udupa J. K., Cho Z. H. and Alavi A. (2013) PET/MR imaging: technical aspects and potential clinical applications. *Radiology* **267**, 26–44.

Toyama H., Ichise M., Liow J. S. *et al.* (2004) Absolute quantification of regional cerebral glucose utilization in mice by ^{18}F-FDG small animal PET scanning and 2-^{14}C-DG autoradiography. *J. Nucl. Med.* **45**, 1398–1405.

Weber B., Burger C., Biro P. and Buck A. (2002) A femoral arteriovenous shunt facilitates arterial whole blood sampling in animals. *Eur. J. Nucl. Med. Mol. Imaging.* **29**, 319–323.

Yu A. S., Lin H. D., Huang S. C., Phelps M. E. and Wu H. M. (2009) Quantification of cerebral glucose metabolic rate in mice using ^{18}F-FDG and small-animal PET. *J. Nucl. Med.* **50**, 966–973.